

Photonic Dipole Contours

Michael Snyder
Murray State University,
Department of Engineering and Physics
Murray State University, Murray, KY 42071
sirzerp@gmail.com

Jonathan Frederick
Murray State University,
Department of Engineering and Physics
Murray State University, Murray, KY 42071
pzadok@gmail.com

Abstract

Understanding magnetic fields is important to facilitate magnetic applications in diverse fields in industry, commerce, and space exploration to name a few. Large electromagnets can move heavy loads of metal. Magnetic materials attached to credit cards allow for fast, accurate business transactions. And the Earth's magnetic field gives us the colorful auroras observed near the north and south poles.

Magnetic fields are not visible, and therefore often hard to understand or characterize. This investigation describes and demonstrates a novel technique for the visualization of magnetic fields. Two ferrofluid Hele-Shaw cells have been used to facilitate the imaging of magnetic field lines [1,2,3,4]. We deduce that magnetically induced photonic band gap arrays similar to electrostatic liquid crystal operation are responsible for the photographed images and seek to mathematically prove the images are of exact dipole nature. We also note by comparison that our photographs are very similar to solar magnetic Heliosphere photographs.

1. Introduction

We seek to analyze the paths that light follows when injected orthogonally into a ferrofluid Hele-Shaw cell (also referred to as “the lens” in this paper). Each cell is made of two circular, optically flat, windows of glass sandwiched together with a very thin layer of ferrofluid in between. Light is injected radially into the edges at regular intervals (various wavelengths have been examined). We define the flat plane of the glass as the xy plane; the light was injected into the outside edges of the glass, and the pictures were taken by a camera in the z axis.

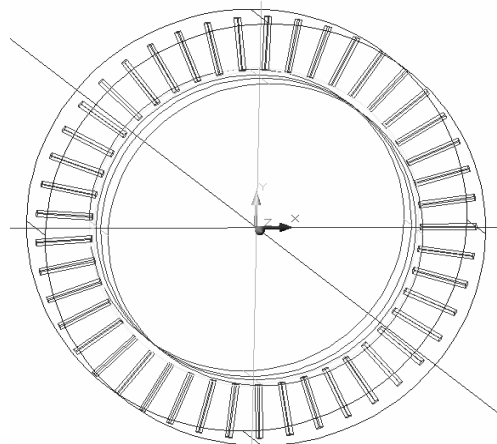


Figure 1: Diagram of lens mount. The radial lines are holes within the apparatus, for light injection.

Two versions of the apparatus were utilized. One was made up of two 150mm diameter BK7 glass windows with a parallelism of 1 arc minute. The second was made up of two 114mm diameter windows that had a hole of 38mm removed from the centers. Both were filled with ferrofluid EFH1 which uses light mineral oil as a continuous medium.

The magnets used for the photographs were 25.4mm diameter tesla rated spherical neodymium-iron-boron magnets mounted on wood dowels and rotated by computer controlled stepper motors. The experimental setup is shown in the supplemental images (Figure 6).

2. Background information

All measurements were kept in pixels. Our goal was to identify the dipole nature contained within our photographs. To define a dipole one needs only the location of one of the poles and the distance vector to the other pole.

The ferrofluid Hele-Shaw cells were made by Timm Vanderelli from Ligonier, Pennsylvania. Mounts and lighting systems were created to investigate his claim of an optical presentation of magnetic flux [2]. In the course of this investigation seven apparatus with different lighting systems and lens sizes have been evaluated. The

trend has been to use larger apparatus with higher resolution cameras. Nine of our resulting videos have been posted on YouTube.com [5].

Both fiber optics and light emitting diodes have been used to inject photons into the lenses. A microscopic image of the particles flowing in the ferrofluid is shown in Figure 2.

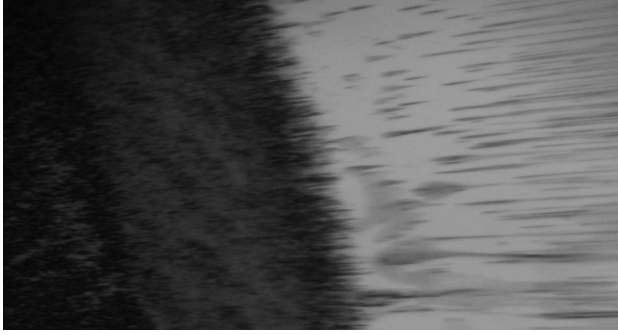


Figure 2: Image of alignment of ferrofluid particles in the presence of a static magnetic field. The dark area at left is the magnet [6].

The illumination leads to two different color response modes of the lenses. Starting at red wavelengths and working down to green wavelengths, photons pass through the lens giving detailed dipole contour lines of the externally imposed magnetic field, as seen in Figure 3.

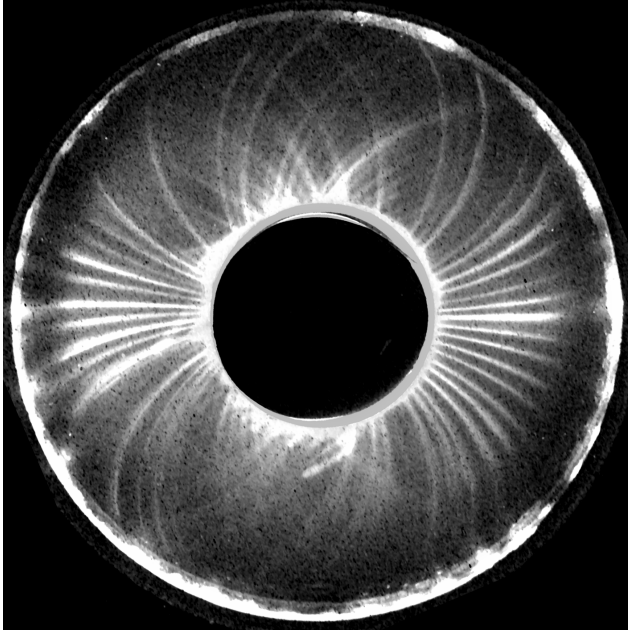


Figure 3: Image taken with red light and vertical dipole moment. The outside edges are light sources.

Blue wavelengths provide significantly different pictures. The blue light images tend to form an evenly

highlighted background, and imposing a magnetic field seems to restrict the amount of light oriented toward the viewer, particularly near the pole locations, leaving a uniform blue field with black void features. As a result, red LEDs were generally used to view dipole field details; and blue LEDs were used to map general pole locations.

Lasers were found to create images but tended to give irreproducible results. Most likely, this is due to the limitations of our equipment. We have found that directed but diffuse light works best for our apparatus.

3. Mathematical Background and Method of Analysis

It has been observed that light “follows” magnetic potential contours in the apparatus under investigation. To see the functional form of magnetic potential lines, it is useful to model our magnets as a single dipole. To begin, the magnitude of the magnetic field of a “magnetic charge” is inversely proportional to the square of the distance from the source and in a direction directly toward or away from it.

$$\vec{H} = \frac{p}{\pi \mu_0} \frac{\vec{r} - \vec{r}_0}{|\vec{r} - \vec{r}_0|^3} \quad (1)$$

In equation (1), H is magnetic field vector, p is the magnetic charge, μ_0 is the permittivity of free space, \vec{r} is the position vector, and \vec{r}_0 is the location vector for the magnetic charge [7]. The constants are uninteresting in our case because it is the geometry that we wish to match; so they will be considered unity from this point forward. In a planar Cartesian coordinate system,

$$\vec{r} = x \vec{i} + y \vec{j} \quad (2)$$

$$\vec{r}_0 = c \vec{j} \quad (3)$$

where the pole is at $(x,y)=(0,c)$. The principle of superposition applies for magnetic fields so the field for a dipole (a north and south pole at a finite separation) is just the sum of their respective fields:

$$\vec{H}_{dipole} = \frac{(x \vec{i} + (y-c) \vec{j})}{|\vec{r} - \vec{r}_0|^3} - \frac{(x \vec{i} + (y+c) \vec{j})}{|\vec{r} - \vec{r}_0|^3} \quad (4)$$

$$|\vec{H}_{dipole}| = \frac{1}{x^2 + (y-c)^2} - \frac{1}{x^2 + (y+c)^2} \quad (5)$$

Equation (4) represents a north pole above the x-axis and a south pole below the x-axis. From all experiments this

does not represent our image, in that we do not record curves of equal H_{dipole} magnitude, but rather curves rotated by $\frac{\pi}{4}$ rad about the z axis to it. The center offset c is half the distance between the two magnetic charges. Our method of comparison assumes there exists an idealized dipole oriented perpendicular to the magnet. This is similar to a magnetic potential field, since the flux lines are nearly circles (it can be shown that circles arranged in this fashion are mutually perpendicular when rotated $\frac{\pi}{4}$ rad). Curves of constant H_{dipole} for various values of c (as in Equation (5)) were computed in MatLab and the experimental images were compared also using MatLab.

4. Data Acquisition

The still photographs were taken with a Nikon 995 digital camera and the movies with a CoVi CVQ-2110 security camera. The CoVi provided an excellent low light NTSC output that was captured onto our lab computer. The Nikon 995 is one of the better low cost cameras for scientific purposes because its exposure and focus settings are lockable during operation providing for a consistent series of photographs. We used a Nikon Wide Angle WC-E63 lens in order to gather as much light as possible. Our best still images came from an exposure setting of 8 seconds and a 4.6 F-stop.

The still photographs were calibrated by using standard astronomical techniques of taking five dark frames before and after every run. The dark frame average was then subtracted from each photograph as it was processed within MatLab.

Our processors of choice were MatLab for images and the program VirtualDub by Avery Lee for the video editing [8]. The standard processing was to break up the photographs and videos into RGB layers and process each layer separately. Contrast and lighting settings were chosen to enhance the dipole lines contained within the images. At no time was information added to photographs; but video filters were used to remove unwanted information. For example, in VirtualDub, the b&w, smoothing, and level filters were used in the videos.

In MatLab the still photographs were broken up into RGB arrays, with dark frame noise subtracted. Then contrast was set by multiplying the arrays by a scalar value. A radial light intensity distance dependence was found within the photos.

The centers of the photographs were brighter than the light sources at the edges. This made digitizing the images challenging because near the center there was one signal to noise ratio, but the levels just a few hundred pixels away were different, meaning any digitizing operation in

Matlab would fail because the photos didn't have consistent signal and noise levels.

This challenge was overcome by multiplying the value of each pixel by 1.02 times its pixel distance away from the center. This equalization process allowed us to create binary masks from the photographs.

5. Data Analysis

Observation of the resulting images suggested that the lines were most likely lines of equal magnetic field of a dipole oriented perpendicular (in the xy plane) to the magnet's actual dipole moment. To confirm this we chose a parameter variation method to find the dipole locations. Our method was to examine the first 24 photographs of a particular run and guess the possible locations of the poles. From this set of initial conditions, a calculation of the associated magnetic field for that pole location could be produced. A computer algorithm was written to vary the locations of the initial guess in an iterative process until a best fit was obtained in comparing the simulation to the observed set of field lines.

To generate the idealized dipole plots, an array was created and filled with inverse square values radiating away from the center. To make a dipole plot, a smaller section of the pole (inverse square) array was taken and then subtracted by an offset section of the same array. The resulting array is a dipole array. To make it easier to work with we deleted the near field values and used the absolute values of the array.

The computer then tagged regions of equal field magnitude values. For example, in MatLab one can issue a single command that finds all the .002 values in the complete array and changes them into 10^{99} values. Then one can digitize all values greater than 10^{98} to ones and all else to zeros. This produces a very quick and accurate equal field line image.

In order to identify those equal potential lines of interest, it was decided to seed the ideal dipole image with equal field magnitude locations from the photographs. This is equivalent to an array indexing operation in a sense, to find a white spot on the original, and then look at the same location on the candidate image array and find the value underneath it. We then tagged all those values in the idealized image equal to the seed-referenced value as in Figures F1-F4. Since both the original and idealized images are made up of curves, the chances of tagging a wrong line and finding an image comparison fit is very small. If one tags the incorrect line, it simply curves away from the area of interest.

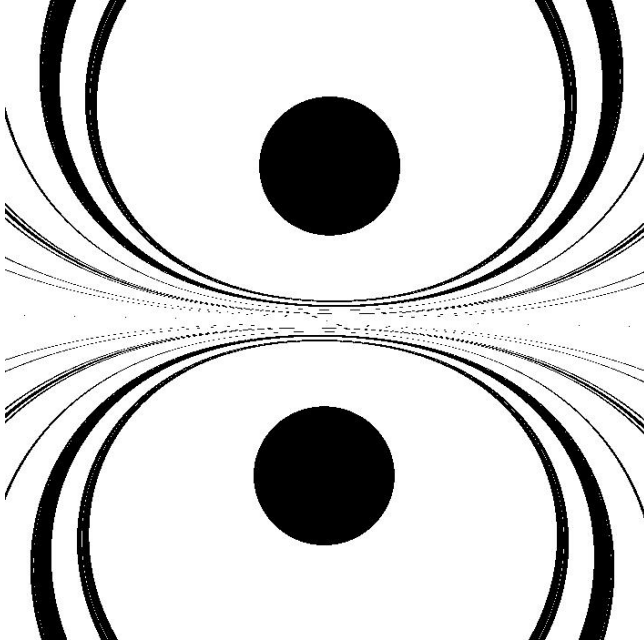


Figure 4: This is an example of the model produced in MatLab.

Only when both the computer generated pole parameters and the correct equal field lines are tagged does the computer return a fit. The best fit is the fit that most closely resembles the experimental image, i.e. the most tagged points. See Figure 4 (and supplemental images S1-S4) for an example of a best fit.

6. Results

After using MatLab to find the best C for 24 representative experimental images we found that

$$C=325\pm 9 \text{ pixels (95\%)}$$

which is approximately twice the diameter of our magnets. C here is twice as much as the c used earlier (in Equation 5) and represents the distance between north and south poles observed with our apparatus. Table 1 shows how our measured C value was arrived at. The x_s and y_s were the best fits that were determined by MatLab. C is just the distance from (x_1, y_1) to (x_2, y_2) .

Table 1: Results of parameter variation in MatLab.

| Image | x_1 | y_1 | x_2 | y_2 | C |
|-------|-------|-------|-------|-------|-------|
| 1 | 547 | 706 | 869 | 701 | 322.0 |
| 2 | 547 | 709 | 871 | 709 | 324.0 |
| 3 | 547 | 704 | 871 | 709 | 324.0 |
| 4 | 547 | 704 | 870 | 709 | 323.0 |
| 5 | 541 | 706 | 870 | 702 | 329.0 |
| 6 | 542 | 704 | 870 | 704 | 328.0 |
| 7 | 546 | 705 | 865 | 701 | 319.0 |
| 8 | 547 | 707 | 865 | 703 | 318.0 |
| 9 | 542 | 702 | 869 | 707 | 327.0 |
| 10 | 540 | 702 | 871 | 708 | 331.1 |
| 11 | 547 | 704 | 871 | 708 | 324.0 |
| 12 | 547 | 705 | 871 | 702 | 324.0 |
| 13 | 547 | 709 | 867 | 702 | 320.1 |
| 14 | 546 | 709 | 871 | 709 | 325.0 |
| 15 | 539 | 707 | 871 | 707 | 332.0 |
| 16 | 547 | 701 | 864 | 709 | 317.1 |
| 17 | 547 | 708 | 871 | 706 | 324.0 |
| 18 | 547 | 709 | 871 | 709 | 324.0 |
| 19 | 539 | 706 | 871 | 706 | 332.0 |
| 20 | 546 | 708 | 871 | 701 | 325.1 |
| 21 | 539 | 707 | 871 | 701 | 332.1 |
| 22 | 539 | 703 | 863 | 702 | 324.0 |
| 23 | 539 | 703 | 863 | 702 | 324.0 |
| 24 | 539 | 707 | 868 | 706 | 329.0 |

In addition to the curves actually analyzed, there exist other orientations of the magnet, all basically consistent with the “following” of equal field lines. This is seen when it is taken into account that magnetic fields are actually extant in three dimensions, instead of the two that have been investigated.

Also, when light is supplied in other orientations, i.e. the room light, a different result is seen. In this case a “bow shock” shape as in Figure 8 is seen, basically concave away from the direction of the light source. Superposition of the two effects is valid, as seen in Figure 9. Also, the images behave as light following dipole surfaces in a limited area of the lens. In the areas adjacent to where the actual north and south poles of the magnet exist, it is seen crossing of light paths. This is contradictory to a simple dipole model or any magnetic field that could exist based on its inverse square without twisting the field. The crossing lines do however bear an uncanny resemblance to those of the sun’s corona [9,10], as shown in Figure 5. Some kind of three dimensional effect may be the cause of this unusual feature.

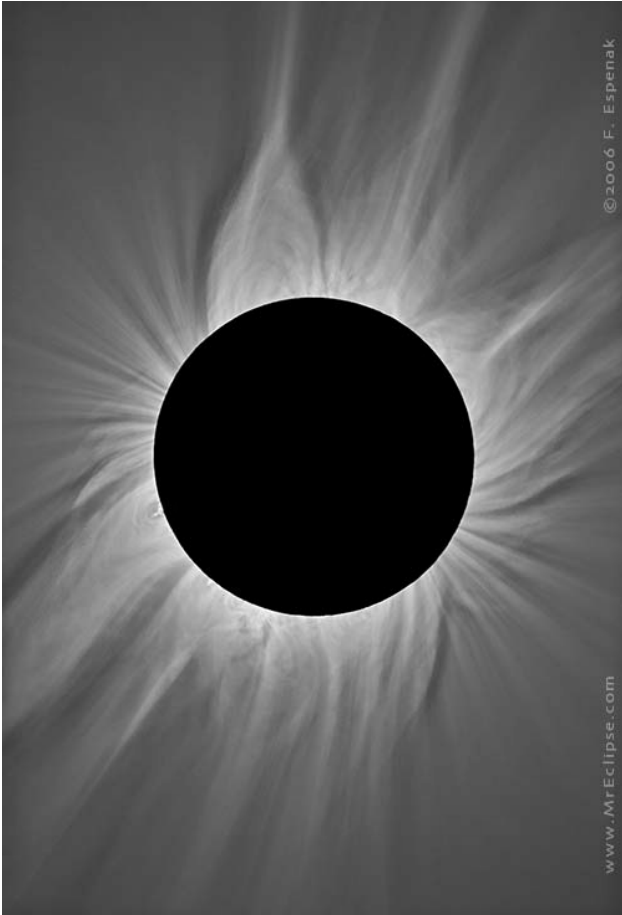


Figure 5: A coronagraph of the solar magnetic heliosphere [9]. Compare with Figure 3.

7. Conclusions

Ferrofluid Hele-Shaw cells are useful as a magnetic field visualization instrument, unlike any other known to the authors. It is quite conceivable that other utilizations will be found with further research of this previously unknown phenomenon [11]. Many questions have been raised during our current research including the magnetic field strength required for the phenomenon to occur and the actual mechanism by which it occurs. Some articles that may help with a mechanisms include [12,13,14].

The mechanism we propose is one of magnetically induced photonic band gap arrays similar to electrostatic liquid crystal operation [15]. The main idea being that the rod like Ferrofluid molecules dynamically line up head to tail like reflective compass needles and form three dimensional waveguides that direct the radially injected light along the surfaces of the dipole.

References

- [1] R.E. Rosenweig, Ferrohydrodynamic Instabilities: Labyrinthine Instabilities. *Ferrohydrodynamics* (1985). pp. 208-16.
- [2] Timm Vanderelli from Ligonier, Pennsylvania. USPTO patent application #20070241745 Magnetic Flux Viewer. <<http://nanomagnetics.us/>>
- [3] R.E. Rosenweig, Magnetic Fluids. *Ferrohydrodynamics* (1985). pp. 33-73.
- [4] C. Sherer and A. M. Figueiredo Neto. Ferrofluids: Properties and Applications. *Brazilian Journal of Physics*, September 2005, pp. 718-27.
- [5] Michael Snyder (2006-2007) <<http://www.youtube.com/user/SirZerp>>.
- [6] Copyrighted Photo by John R. Shearer of Pittsburgh (10/2007)
- [7] R.E. Rosenweig. Electromagnetism and Fields: Magnetostatic Field Equations. *Ferrohydrodynamics* (1985). pp. 74-77.
- [8] VirtualDub by Avery Lee <<http://virtualdub.sourceforge.net/>>.
- [9] Copyrighted Photo by Fred Espenak <<http://www.mreclipse.com/MrEclipse.html> >.
- [10] Solar and Heliospheric Observatory Website. <<http://sohowww.nascom.nasa.gov/>>.
- [11] Alfonso F. Davila. Detection and Function of Biogenic Magnetite. pp. 61-79.
- [12] Richard J. Cook, Heidi Feam, and Peter W. Milonni. Fizeau's Experiment and the Aharonov-Bohm Effect. *American Journal of Physics*, August 1995, pp. 705-10.
- [13] John P. McTague. Magnetoviscosity of Magnetic Colloids. *The Journal of Chemical Physics*, July 1969, pp. 133-6
- [14] W.F. Hall and S.N. Busenberg. Viscosity of Magnetic Suspensions, *The Journal of Chemical Physics* July 1969, pp. 137-44.
- [15] Gerhard Meier. *Applications of Liquid Crystals* (1975).

Open Dataset Download Links

For the casual reader I would recommend the <http://www.youtube.com/user/SirZerp> link to see our lab work. If you have a scientific interest in our videos, I am providing links of higher resolution videos via a download service for a limited amount of time.

If the links do not work, or if you would like uncompressed AVI files, email me at sirzerp@gmail.com and I will either provide a newer link or sent you a DVD through the mail. We believe in open datasets and are willing to share our data with anyone who wishes to see it.

This paper and all of our photos and videos are copyrighted by Jonathan Frederick and Michael Snyder (2007). Also the pictures used by permission of John R. Shearer and Fred Espenak are copyrighted respectively.

- 1) I_of_Ellipses.gif www.sendspace.com/pro/wb717
This animated gif shows a magnet being rotated in the xy plane in red light giving detailed lines.
- 2) XYRotate.gif www.sendspace.com/pro/oejyth
This animated gif shows a magnet being rotated in the xy plane in blue light giving detailed pole voids.
- 3) YZRotate.gif www.sendspace.com/pro/qs66mn
This animated gif shows a magnet being rotated in the yz plane in blue light giving detailed pole voids.
- 4) Eye of Ellipses.avi www.sendspace.com/pro/zqykli
This primary video is the highest resolution video of the set; it shows a magnet being rotated in the xy plane in red light giving detailed lines.
- 5) Invertedquadsmall.avi www.sendspace.com/pro/ng5xei
This primary video was done during the summer with an older 100mm apparatus testing out the new stepper motors. It shows two magnets in the xy plane producing a quadrupole dipole field.
- 6) Shuntvortex www.sendspace.com/pro/l71j1u
This small video is the strangest of the lot. Two rod shaped magnets were embedded into wood dowels in a repulsive configuration with the poles facing the camera. The dowels were rotated by a drill; I have provided all three colors.
- 7) Seven www.sendspace.com/pro/9p9mxf
This is a secondary video showing a magnet moved around the apparatus by hand.
- 8) BrokenwithPolePictures.avi www.sendspace.com/pro/vx40te
This is a time lapse video with pictures taken every 20 seconds for four hours. The apparatus had been damaged. This video was shot merely for curiosity purposes. Every 100 frames the magnet is flipped, with the poles facing the camera.
- 9) Bluetornadoes www.sendspace.com/pro/fu1jjw
Source video for Shuntvortex video. It shows a 'tunnel' connection between the magnets for 10 minutes.

Supplemental Image Gallery



Figure 6: The experimental setup showing camera in a box and lens on the left face of the box. During operation, the box is closed, and the room lights usually turned off.

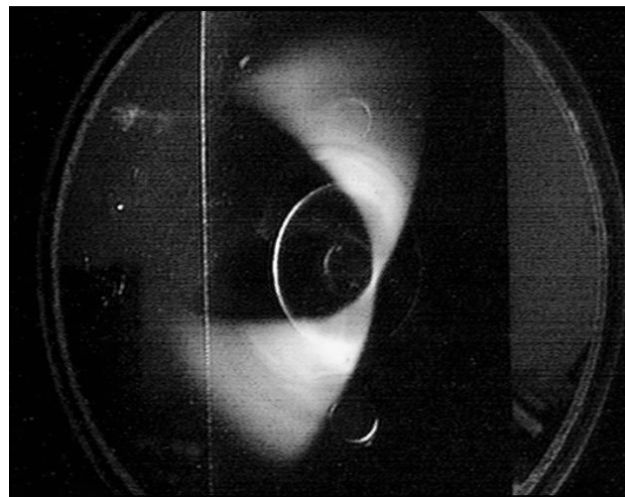


Figure 8: Photograph of a pronounced “bow” with white light source to the right (not visible) and dipole moment on the z-axis. Annular magnet at center.

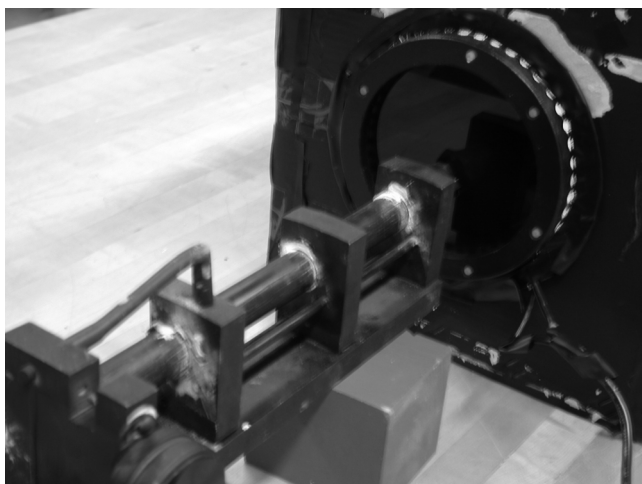


Figure 7: The apparatus showing the magnet location and use of stepper motor mounted on a PVC frame. Blue LEDs were used in this case



Figure 9: Photograph of a “bow” effect with white light source to the right (not visible) and blue LEDs turned on. Two repulsive dipole moments on the z-axis.

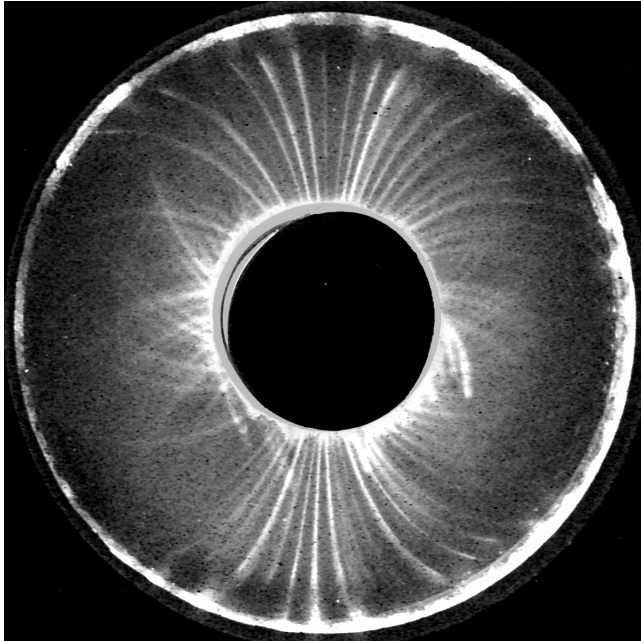


Figure S1: Source image #6

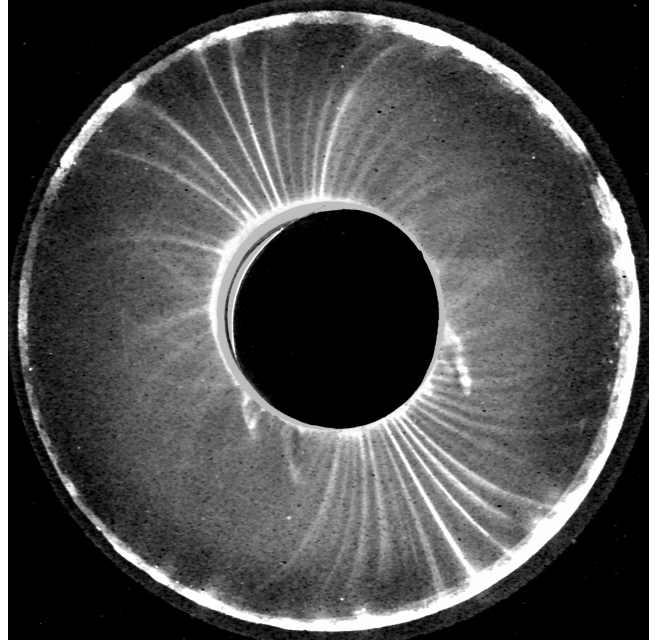


Figure S2: Source image #19

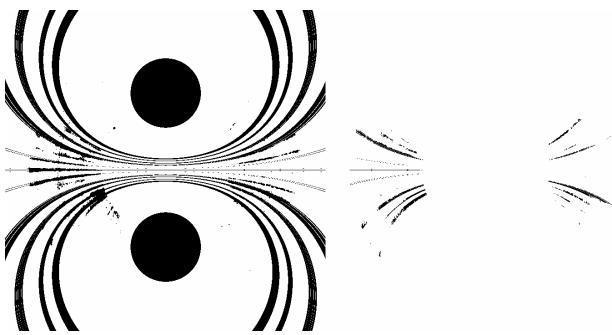


Figure F1: Fit of image #6 rotated 88 degrees,
(experimental mask | idealized dipole) on Left
(experimental mask & idealized dipole) on Right

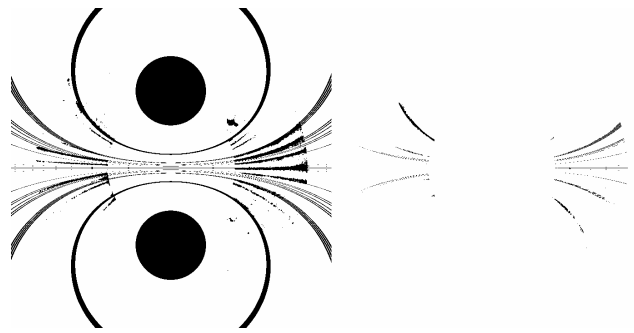


Figure F2: Fit of image #19 rotated 299 degrees,
(experimental mask | idealized dipole) on Left
(experimental mask & idealized dipole) on Right

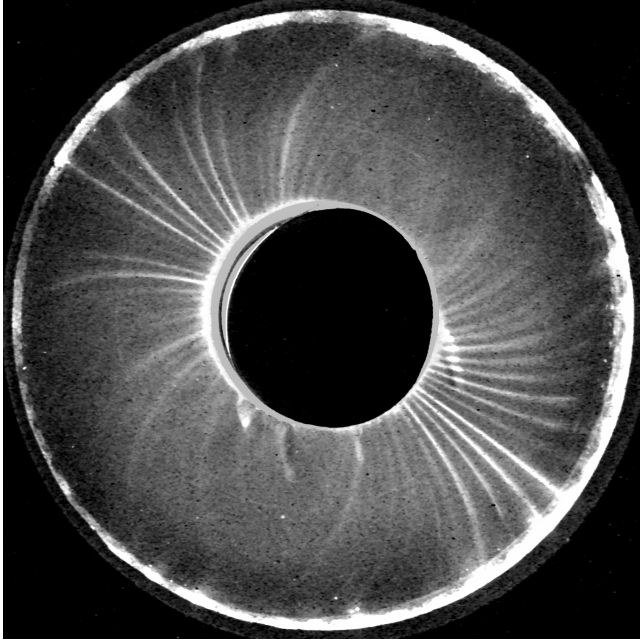


Figure S3: Source image #21

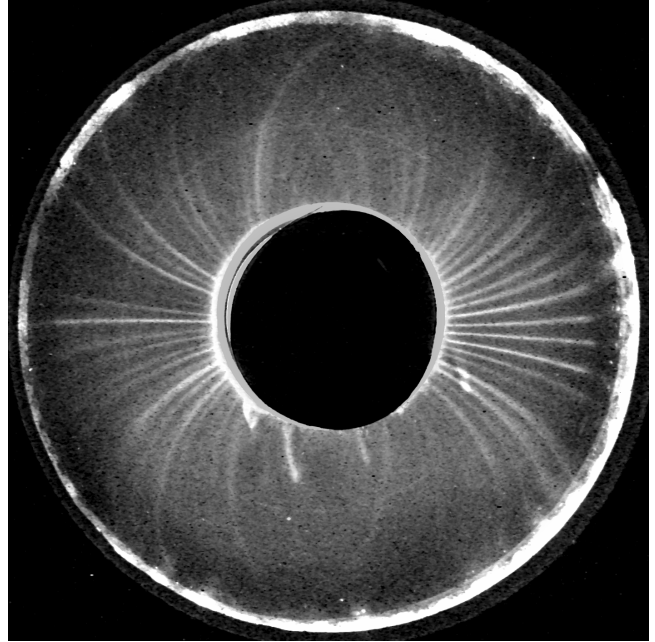


Figure S4: Source image #23

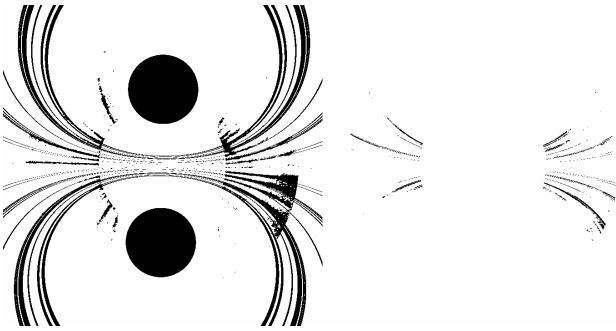


Figure F3: Fit of image #21 rotated 330 degrees,
(experimental mask | idealized dipole) on Left
(experimental mask & idealized dipole) on Right

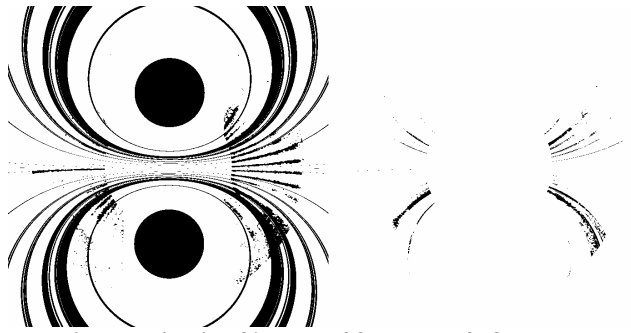


Figure F4: Fit of image #23 rotated 358 degrees,
(experimental mask | idealized dipole) on Left
(experimental mask & idealized dipole) on Right